24 October 2022

Molecular Basis for Interferon-mediated Pathogen Restriction in Human Cells

Sumit K. Matta[1], Hinissan P. Kohio[1a], Pallavi Chandra[2a], Adam Brown[3], John G. Doench[3], Jennifer A. Philips[1,2], Siyuan Ding[1], L. David Sibley[1]*

[1]Department of Molecular Microbiology, School of Medicine, Washington University in St. Louis, St Louis. MO 63130

[2]Department of Medicine, Division of Infectious Diseases, School of Medicine, Washington University in St. Louis, St Louis. MO 63130

[3]Broad Institute of Harvard and MIT, Cambridge, MA, 02142

[a] contributed equally

*Correspondence: sibley@wustl.edu

Key words: Interferon gamma, Toxoplasma, Mycobacteria, anti-viral immunity, STAT1, ubiquitin ligase, RNF213, CRISPR/Cas9, genome-wide screen

Abstract

To define novel mechanisms for cellular immunity to the intracellular pathogen *Toxoplasma gondii*, we performed a genome-wide CRISPR loss-of-function screen to provide an unbiased assessment of genes important for IFN-γ-dependent growth restriction. We revealed a previously unknown role for the tumor suppressor NF2/Merlin for maximum induction of Interferon Stimulated Genes (ISG), which are positively regulated by the transcription factor IRF-1. We then performed an additional focused ISG-targeted CRISPR screen that identified the host E3 ubiquitin ligase RNF213 as essential for IFN-γ mediated control of *T. gondii*. RNF213 mediated ubiquitination of targets on the parasite-containing vacuole and growth restriction in response to IFN-γ in a variety of cell types, thus identifying a conserved factor that plays a prominent role in human cells. Surprisingly, growth inhibition did not require the autophagy protein ATG5, indicating that RNF213 initiates restriction independent of a non-canonical autophagy pathway that has previously been implicated in control of *T. gondii*. RNF213 was also important for control of unrelated intracellular pathogens in human cells treated with IFN, as shown here for *Mycobacterium tuberculosis* and Vesicular Stomatitis Virus. Collectively, our findings establish RNF213 as a critical component of cell-autonomous immunity to a broad spectrum of intracellular pathogens in human cells.

Introduction

Toxoplasma gondii is a widespread parasite of animals that also frequently causes zoonotic infection in humans. As an obligate intracellular parasite, *T. gondii* resides within a specialized vacuole that is largely sequestered from the host endomembrane system (1), which the parasite protects to provide niche for intracellular growth (2, 3). Cell autonomous mechanisms for immune control of intracellular *T. gondii* are best known from studies in the natural murine host, for which laboratory rodents are a useful model (4, 5). Type II interferon, or interferon gamma (IFN-γ), plays the major role in resistance to infection in mouse (6, 7), while type I interferon is also produced and contributes to control of infection (8), particularly in the central nervous system (CNS) during chronic infection (9). Treatment with IFNs leads to upregulation of numerous Interferon Stimulated Genes (ISGs), the exact complement of which varies by cell type (10, 11). Among the most strongly upregulated ISGs are the critically important immunity related GTPases (IRGs) and guanylate binding proteins (GBPs), which collectively lead to vacuole rupture, parasite destruction, and clearance (12-14). The IRG/GBP system is under control of a noncanonical autophagy (ATG) system that requires core ATG components for conjugation of LC3 to phosphatidyl ethanolamine (PE), but it does not require the initiation nor

57 degradative steps (15-17). Although, IRGs and GBPs play a central role in immunity in rodents,
58 human cells largely lack IRGs and GBPs have been described to play a more limited role, as
59 discussed further below.
60 Clinical evidence that human cells control intracellular *T. gondii* via an interferon-mediated
61 process comes from studies demonstrating that immunocompromised patients with low levels of
62 IFN-γ are susceptible to reactivation of latent toxoplasmosis (18, 19). In vitro studies indicate
63 that multiple IFN-γ-dependent pathways can mediate growth restriction in humans. Although
64 humans are not natural hosts in the life cycle, human macrophages are nonetheless able to
65 control the replication of intracellular *T. gondii* in response to IFN-γ (20, 21) and IFN-β (22, 23).
66 Nonhematopoietic human cells also control intracellular *T. gondii* through varied and often cell-
67 type specific mechanisms (24). For example, induction of indole amine oxidase (IDO) by
68 interferon leads to degradation of tryptophan, thus limiting parasite growth in human fibroblasts
69 (25) and human brain microvascular endothelial cells (26). In addition, the noncanonical
70 autophagy pathway described above is required for recruitment of LC3, leading to engulfment of
71 the parasite containing vacuole in multiple membranes, a process that is associated with growth
72 restriction in Hela cells (27), A549 cells (28), and human umbilical vein endothelial cells (29).
73 Curiously, the ATG-dependent growth restriction is not global (16), but rather limited to those
74 vacuoles that become ubiquitinated and acquire adaptors such as p62, NDP52, and LC3 (27,
75 29). Virulent type I strains are largely resistant to this pathway, while types II and III are
76 susceptible (27), although the basis for this difference is unknown. Recent studies identified the
77 E3 ubiquitin ligase RNF213 as a candidate for mediating early ubiquitination of *T. gondii*-
78 containing vacuoles in IFN-γ treated A549 cells (30). The IFN-γ signaling and noncanonical ATG
79 pathways are partially connected by ISG15, which is required for maximal recruitment of ATG
80 adaptors and also interacts with RNF213 (28). Additionally, GBP1 has been implicated in
81 restricting *T. gondii* growth in human epithelial cells, despite not being recruited to the vacuole
82 (31), while it is recruited to the vacuole membrane in THP-1 cells, resulting in rupture and
83 activation of apoptosis (32). Additionally GBP2 and GBP5 contribute to growth restriction in
84 THP-1 cells, despite not being recruited to the parasite containing vacuole (33). Collectively,
85 these prior candidate-gene studies indicate that multiple IFN-γ–dependent mechanisms can
86 contribute to growth restriction, which is often partial and expressed in a cell-specific manner.
87 However, the absence of any prior global or unbiased assessment of genes required for IFN-γ
88 mediated growth restriction leaves open the possibility that a previously unrecognized, IFN-γ-
89 mediated pathway exists in all or most human cells.

90 To provide an unbiased assessment of the predominate pathways for control of *T. gondii*
91 growth in IFN-γ activated human cells, we performed genome-wide CRISPR screen in A549
92 cells. Our findings reveal a previously unanticipated role for the tumor suppressor NF2 in
93 modulating IRF-1-dependent gene expression, hence dampening ISG expression. Additionally,
94 an ISG-focused CRISPR screen identified the E3 ligase RNF213 as an essential component of
95 control of *T. gondii* in multiple human cell lines treated with IFN-γ. Surprising, although RNF213
96 was associated with ubiquitination and recruitment of ATG adaptors including LC3, it functioned
97 independently of the previously described pathway for non-canonical autophagy. Moreover,
98 RNF213 exerted a general antimicrobial activity against intracellular bacteria and viruses,
99 including *Mycobacterium tuberculosis* and vesicular stomatitis virus, revealing a conserved role
100 in cell autonomous immunity in human cells.
101

102 ## Results

103 **Genome-wide CRISPR screen identifies factors important for IFN-γ mediated growth**
104 **restriction**

105 Although depletion of tryptophan due to induction of IDO has been described as a mechanism
106 for restricting growth of *T. gondii* in some cell types (24), we previously reported that disruption
107 of the IDO gene in A549 cells has no impact on IFN-γ mediated growth restriction (34).
108 Consequently, we selected A549 cells to define novel mechanisms for IFN-γ mediate growth
109 restriction based on CRISPR-mediated loss of function screens. Initially, we validated the
110 growth restriction following IFN-γ activation of A549 cells using a previously described vacuole
111 size assay (9). We used the type III strain named CTG of *T. gondii* as it is highly susceptible to
112 growth restriction, relative to either type I or type II strains (27, 35). The vacuole size assay
113 takes advantage of the fact that parasite replication leads to increased size of the vacuole while
114 growth inhibition by IFN-γ blunts the expansion of parasites. Quantification of vacuole size after
115 IFN-γ treatment verified that wild type (WT) cells restricted parasite expansion and that this
116 ability was IFN-γ dependent, as shown by loss of growth restriction in STAT1 knockout (STAT1-
117 KO) cells (**Fig. 1A, Fig. S1A**). As expected, the growth restriction was independent of
118 exogenously added tryptophan, indicating it does not rely on IDO1, even though this gene is
119 induced in IFN-γ treated A549 cells (34). To develop a process for selecting cells from the
120 population, we infected A549 cells with a recombinant CTG strain expressing GFP (CTG-GFP),
121 trypsinized cells from the dish, and analyzed them by flow cytometry to evaluate the average
122 intensity of GFP as a proxy for parasite growth (**Fig. 1B**). Although there was not a distinct

separation between the populations of CTG-GFP in WT vs. STAT1-KO cells, there was a clear shoulder of higher GFP expression in the STAT1-KO cells (green box, **Fig. 1B**). We therefore reasoned that escape mutants that lose the ability to control parasite replication should mimic the growth of CTG-GFP in STAT1-KO cells, thus providing the basis for the CRISPR-based screens described below.

We then used lentiviral transduction of A549 cells to express the Brunello library containing 4 guides each to ~20,000 genes in the human genome (36) and developed a screen for loss of IFN-γ mediate growth restriction (**Fig. 1C**). We scaled the culture assays to aim for single sgRNA per cell with ~ 100x coverage of each gene such that loss of guides during expansion could be quantified. Cells were expanded for 8 passages to allow for stabilization of the population of guides that did not affect viability. Cells were then activated with IFN-γ, infected with CTG-GFP, and the top 5% of GFP expressing cells were sorted from four independent experiments (**Fig. 1D**). The sgRNAs from these pools were amplified, barcoded, and subjected to NGS sequencing using the Illumina platform. We reasoned that sgRNAs that are enriched in the top 5% pool represent genes whose loss results in impaired IFN-γ mediated growth restriction of CTG-GFP. Comparison of the guide abundances in the top 5% relative to a time-matched point for the uninfected pool was used to classify guides that were significantly different based on Fold Change and FDR (False Discovery Rate) in the four replicates of the primary screen (**Fig. 1E**, **Dataset 1**). There was a high degree of variability in genes that were scored significant between the various replicates. For example, only 5 genes (including NF2, FRYL) met the individual *P* value for significance in all 4 replicates when analyzed separately (**Fig. S1B**). Additionally, 23 genes were individually significant in 3 of 4 while 224 were significant in 2 of 4 replicates (**Fig. S1B**). However, using the more stringent criteria of FDR for the combined replicates, only NF2 and FRYL were scored as significant (**Fig. 1E**). Although guides for STAT1 and IRF1 were slightly enriched, the strongest signal for enhanced sgRNA guides correspond the gene NF2 (Neurofibromatosis 2) an Ezrin / Radixin / Moesin (ERM) family member that is also known as MERLIN (37), and which functions as a tumor suppressor (**Fig. 1E**). We also detected three genes that showed depletion of sgRNAs (PTEN, TSC1 and TSC2) (**Fig. 1E**). Although we have not followed up on these hits, they presumably are depleted because cells lacking these genes have decreased survival during infection and IFN-γ treatment.

Secondary pool CRISPR screen identifies IFN-γ-STAT1 axis and NF2 as critical for growth restriction

156 Comparison of the results from the primary screen revealed a high degree of variability in
157 genes classified as significantly different between the replicates, which is not unexpected for
158 FACS-based screens (38). We therefore considered it possible that the genome-wide screen
159 may have missed genes that contribute to IFN-γ mediated resistance. Consequently, we
160 developed a secondary screen based on a pool of genes that were significantly enriched in at
161 least 2 of 4 replicates of the primary screen (**Fig. S1B**). The secondary screen included 224
162 genes with coverage of 10 sgRNAs per gene, thus improving statistical power for identifying
163 differences. The secondary screen identified several factors in the IFN-γ-STAT1 axis; their loss
164 suggests that they are essential for growth restriction **(Fig. 1F**) (**Dataset 2**). Included in the set
165 of highly enriched guides representing depleted genes were STAT1, the JAK2 kinase that
166 phosphorylates STAT1, the IFN-γ receptor subunits IFNGR1 and IFNGR2 as well as the
167 downstream transcription factor IRF-1, which augments the activity of IFN-γ on inducing gene
168 expression (39) (**Fig. 1F**). The only gene not part of the IFN-γ-STAT1 pathway was NF2, which
169 was the top hit in the primary screen (**Fig. 1F**). The four other genes that were significantly
170 enriched in each replicate of primary screen, including FRYL, were not enriched in the T5
171 population of the secondary screen.
172 NF2 has previously been implicated in suppressing tumors via interaction with the E3
173 ubiquitin ligase CRL4 in the nucleus (37), and in regulating mTOR (40) and modulating
174 metabolism (41); however, it has not previously been associated with IFN-γ activation nor
175 pathogen control. To elucidate its contribution to cell-autonomous pathogen control, we
176 generated KOs using lentiviral transduction and targeted CRISPR-Cas9 gene editing for both
177 NF2 and IRF-1 in A549 cells (**Fig. S2**). As expected, IRF-1 showed dependence for expression
178 in WT cells and NF2-KO cells on IFN-γ treatment, while NF2 was not affected by IFN-γ
179 treatment (**Fig. 2A**). We then ascertained the ability of IFN-γ to control growth of CTG parasites
180 in WT, IRF-1 KO and NF2 KO cells using the vacuole size assay. As expected, growth
181 restriction seen in WT cells was completely lost in IRF-1 KO cells, consistent with previous
182 reports that this transcription factor is essential for control of *T. gondii* in IFN-γ treated cells (34).
183 In contrast, loss of NF2 resulted in a partial, yet significant reduction in the growth restriction
184 following IFN-γ (**Fig. 2B and 2C**).
185 **Loss of NF2 down-modulates IRF-1 dependent ISG expression**
186 To better define the role of NF2 in IFN-γ dependent growth restriction, we compared the
187 transcriptional profile of WT, IRF-1 KO and NF2 KO cells under resting and activated conditions.
188 Comparison of the NF2 KO to WT cells revealed multiple of genes that were NF2 dependent

189 (**Fig. S3**), which likely reflect its diverse roles. However, when we compared the IFN-γ induced
190 genes that were IRF-1-dependent, there was a clear pattern that most of these genes were also
191 dampened in the NF2 KO (**Fig. 2D**). The extent of suppression in the NF2 KO varied among
192 genes: for example, APOL3 was IRF-1 dependent but only partially affected by NF2, whereas
193 IDO, GBP4 and RARESS3 were more strongly affected by NF2 as well as IRF-1 (**Fig. 2E**). We
194 also examined the effect of NF2 on IFN-β driven expression using an ISRE (Interferon
195 Stimulation Response Element) promoter normalized to constitutively expressed firefly
196 luciferase. Induction of ISRE activity by IFN-β was significantly lost in both IRF1 KO and NF2
197 KO cells (**Fig. 2F**), indicating that both factors likely also participate in IRF-1 mediated
198 transcription.

199 **ISG targeted CRISPR screen identifies RNF213 as the primary determinant of IFN-γ**
200 **mediated growth restriction in multiple human cell types**

201 We were surprised that neither the primary nor secondary genome-wide screens identified
202 any canonical ISGs, except for the broadly acting transcription factor IRF-1, which affects many
203 ISGs. Consequently, we designed a focused CRISPR screen based on a previous set of ISGs
204 that was defined by transcriptional induction in response to IFN-γ in A549 cells (34). The ISG
205 screen included ~350 genes with coverage at 10 sgRNAs per gene and was repeated four
206 times independently (**Fig. 3A**). Sequencing the top 5% of CTG-GFP positive cells was used to
207 define sgRNAs that were significantly enriched, thus identifying genes important for IFN-γ
208 mediated control. We identified only a single strong positive corresponding the E3 ligase
209 RNF213, in addition to the broadly acting IRF-1 (**Fig. 3B**) (**Dataset 3**). RNF213 is not widely
210 recognized as an ISG due to its constitutive expression in many cell types, and yet it is
211 upregulated by ~ 8 fold in A549 cells treated with IFN-γ and thus was part of the library used in
212 the screen. RNF213 ranked 304 in the primary screen (**Dataset 1**) but did not meet the criteria
213 for the secondary pool screen, although sgRNA guides for this gene were enriched in the top
214 5% population in 3 of 4 replicates by > 2 fold. Given its prominent position in the targeted ISG
215 screen, we decided to examine its function. Deletion of RNF213 resulted in enhanced growth of
216 CTG strain parasite in both untreated cells and it completely reversed the growth inhibition
217 normally seen in IFN-γ treated A549 cells (**Fig. 3C and 3D**). Notably, although sgRNAs were
218 present for IDO1, ISG15, GBP1, and RARRES3, their frequency was not changed in the top 5%
219 pool, indicating the singular loss of these genes does not contribute substantially to IFN-γ
220 mediated growth restriction under the conditions of the screen.

221 Many factors that have been previously described to restrict *T. gondii* growth in IFN-γ treated
222 human cells are either cell type specific or limited to specific parasite lineages (24). To test how
223 widely conserved the function of RNF213 was, we generated KOs in human foreskin fibroblasts
224 (HFF) and in the human monocytic cell line THP-1 (**Fig. S4**). Similar to the situation in A549
225 cells, loss of RNF213 resulted in slightly enhanced growth in untreated HFF cells and a loss of
226 IFN-γ mediated growth inhibition (**Fig. 3E and F**). Additionally, the loss of RNF213 in THP-1
227 cells reversed the inhibition of *T. gondii* growth following treatment with either IFN-γ or IFN-β
228 combined with TNF-α (**Fig. 3G and H**), either of which have previously been shown to control *T.*
229 *gondii* growth (9). Notably, the loss of RNF213 in all three cell types completely reversed the
230 effects of IFN-γ, similar to loss of STAT1 or IRF-1 in A549 cells. Additionally, the expression of
231 RNF213 was sub-maximal in IRF-1 KO and NF2 KO cells treated with IFN-γ (**Fig. S4A**),
232 suggesting they may act through this downstream mediator. Collectively, these findings argue
233 that RNF213 is the major effector downstream of both type I and type II IFNs that inhibits
234 parasite growth in human cells.

235 **RNF213-dependent growth restriction leads to recruitment of autophagy adaptors but is**
236 **independent of ATG5**

237 Consistent with its requirement for growth restriction, RNF213 was recruited to a portion of
238 *T. gondii* vacuoles in untreated cells, and this increased dramatically following treatment with
239 IFN-γ as shown by immunofluorescence assay (IFA) and immuno-EM (**Fig. 4A-C**). Since
240 ubiquitination is thought to be the first step in marking the *T. gondii* vacuole for growth restriction
241 (27), we stained cells with FK2, which recognizes both mono and poly ubiquitin (Ub) chains, in
242 combination with RNF213. The proportion of vacuoles that were FK2 positive closely matched
243 the percentage that were also positive for RNF213, while the number that were RNF213 positive
244 considerably exceeded this value (**Fig. 4C**). The higher percentage of RNF213 positive staining
245 vacuoles, suggesting that RNF213 is initially recruited to the PVM followed by ubiquitination,
246 resulting in double positive vacuoles. Similar co-staining of RNF213 and FK2 was observed in
247 IFN-γ activated HFF and THP-1 cells infected with CTG (**Fig. S5).** Downstream of IFN-γ
248 mediated ubiquitination, the PVM acquires several adaptors, including p62 and NDP52, that
249 recruit the autophagy adaptor LC3 (27-29). Consistent with these previous reports, recruitment
250 of LC3 was low in non-activated cells, and significantly elevated after treatment with IFN-γ (**Fig.**
251 **4D and E**). The proportion of vacuoles that were positive for both FK2 and LC3 was similar,
252 while singly FK2 positive vacuoles considerably exceeded this value (**Fig. 4E**). These
253 differences in positivity suggests that ubiquitination occurs first, followed by recruitment of LC3.

254 Examination of the vacuole membrane surrounding the parasite by TEM revealed that it was
255 often wrapped by numerous membranes (**Fig. 4F**), a phenotype that has previously been
256 associated with growth restriction by non-canonical autophagy (27). Combined with the
257 recruitment LC3, this profile suggested that RNF213 may act to recruit components of the non-
258 canonical autophagy pathway to restriction growth of the parasite. To test this idea, we
259 generated a knockout of ATG5 in A549 cells, and verified its absence by western blotting and
260 loss of conversion of LC3I to the lipidated LC3II form (**Fig. 4G**). Contrary to expectation, loss of
261 ATG5 minimally affected the growth restriction of *T. gondii* in IFN-γ treated cells (**Fig. 4H**). To
262 ascertain whether loss of ATG5 might have affected the recruitment of RNF213 to the parasite
263 containing vacuole, we stained IFN-γ treated and infected ATG5 KO cells for RNF213 and FK2.
264 Similar to WT cells, parasites were frequently labeled by both RNF213 and FK2 in ATG5 KO
265 cells (**Fig. 4I**). Collectively, these findings indicate that RNF213 lies upstream of ubiquitination
266 and that growth restriction requires RNF213 but not an ATG5 dependent process.
267
268 **RNF213 participates in interferon-mediated control of bacterial and viral pathogens**
269 Previous studies have described a role for RNF213 in recognition and ubiquitination of LPS on
270 intracellular *Salmonella* (42). To explore the role of RNF213 in control of intracellular bacteria
271 that do not contain LPS, we examined the requirement for RNF213 in IFN-γ activated A549 cells
272 infected with *Mycobacterium tuberculosis* (Mtb). Human cells normally are not able to clear
273 intracellular Mtb following treatment with IFN-γ but rather restrict their intracellular growth.
274 Consistent with this profile, the colony forming units of Mtb remained static in IFN-γ treated cells
275 grown for 48 h, compared to control cells where they increased significantly (**Fig. 5A**). Loss of
276 RNF213 significantly impaired the ability of IFN-γ to control replication of Mtb (**Fig. 5A**).
277 Immunofluorescence localization also revealed that RNF213 was recruited to the surface of Mtb
278 in A549 cells and that these vacuoles also stained with FK2 indicating that they were
279 ubiquitinated (**Fig. 5B**). RNF213 has also been reported to facilitate control of Rift Valley fever
280 virus, an enveloped segmented RNA virus (43). We also explored the potentially broad anti-
281 microbial role of RNF213 in control of intracellular viral replication using a non-segmented RNA
282 virus. We examined type I IFN (IFN-β) treated A549 cells infected with vesicular stomatitis virus
283 expressing GFP (VSV-GFP). Treatment with IFN-β resulted in a significant decrease in viral
284 replication in WT cells that was reversed in IRF-1 KO and RNF213 KO cells (**Fig. 5C and D**).
285 Collectively, these findings suggest that RNF213 may recognize a host component that is

common to multiple pathogens, rather than a panoply of different molecules each unique to one pathogen.

Discussion

To identify conserved mechanisms of cell autonomous immunity to intracellular pathogens, we performed a genome-wide CRISPR screen for loss of *T. gondii* growth restriction in response to IFN-γ. Although the primary screen failed to identify previous candidate genes implicated in control, we ascribed a new role for the tumor suppressor gene NF2 in upregulating expression of IRF-1 dependent ISGs. To account for the possibility that the primary screen lacked power to identify single gene effects, we performed an ISG-targeted screen for loss of IFN-γ-mediated *T. gondii* growth restriction. The ISG-targeted screen identified the E3 ligase RNF213 as the primary effector important for IFN-γ mediated control of *T. gondii* growth in human cells. RNF213 was upregulated by IFN-γ, recruited to the parasite containing vacuole, and associated with initial ubiquitination of targets at this interface. Deletion of RNF213 revealed that it was necessary for growth restriction, despite not relying on ATG5, which may act at downstream steps independent of growth restriction. Loss of RNF213 also diminished antibacterial and antiviral responses to interferon, suggesting it controls a common host pathway needed for pathogen resistance. These studies define a broad role for RNF213 as an essential mediator of growth restriction of divergent pathogens in a variety of human cell types.

Although previous studies have focused on candidate genes, we were interested in an unbiased method to identify genes important for IFN-γ mediated control of *T. gondii*. To this end, we developed a FACS-based CRISPR-screen to identify genes whose absence results in loss of IFN-γ mediated growth restriction of a GFP-expressing strain of *T. gondii*. The genome-wide CRISPR screen identified a number of components in the STAT1 signaling pathway including JAK2, the receptors IFNGR1 and IFNGR2, and the transcription factor IRF-1. These hits validate the screen as being sufficient to identify factors that globally affect the IFN-γ response. In particular, IRF-1 amplifies the responses normally triggered by engagement of STAT1 on promoters bearing GAS sequences (44), thus upregulating a constellation of ISGs. Consistent, with this ability we found that IRF-1 was necessary for maximal growth control following IFN-γ stimulation. Independently, we have previously shown that overexpression of IRF-1 in A549 cells is sufficient to induce control of *T. gondii* growth (34). We also identified NF2 as a significant hit in the primary genome-wide and pooled secondary CRISPR screens. Consistent with its prominent ranking in the CRISPR screens, deletion of NF2/Merlin significantly reduced the expression of IRF-1-dependent genes ungulated by IFN-γ, in addition to dysregulating

320 numerous unrelated genes. This finding was unexpected as NF2 is known as a tumor
321 suppressor gene that negatively regulates mTOR and the Hippo signaling pathways but is
322 without prior connection to interferon signaling (40, 41). NF2/Merlin binds to and inhibits the E3
323 ubiquitin ligase CRL4 in the nucleus, thereby suppressing tumorigenesis (37). Previous studies
324 have shown that CRL4 ubiquitinate histones and/or transcription factors leading to down-
325 regulated gene expression (45). Hence, it is possible that in the absence of NF2/Merlin, CRL4
326 may target IRF1 to down-regulate its activity. Among the ISGs that are NF2 and IRF-1
327 dependent, RNF213 may factor prominently given its essential downstream role in mediating
328 IFN-γ growth inhibition.
329 Because the genome-wide CRISPR screen failed to find previous candidate genes, we
330 considered it might lack sufficient power to identify such single factors. As such, we performed a
331 targeted CRISPR screen of ISGs that we have previously shown to be upregulated in A549 cells
332 (34). Despite the fact that this screen included a number of previously recognized factors that
333 control IFN-γ mediated growth in other human cells including RARESS3 (34), ISG15 (28), GBPs
334 (32, 33), and IDO (25), these genes were not identified as significant hits. This finding suggests
335 that while these genes have demonstrable effects when tested individually, their individual
336 contributions are too modest to show differences at the population level, at least based on the
337 conditions used here. Instead of these previously characterized factors, the ISG-targeted
338 CRISPR screen identified a prominent role for RNF213, which is expressed at basal levels and
339 upregulated in response to IFN-γ (34). RNF213 was essential for IFN-γ mediated restriction of *T.*
340 *gondii* growth in multiple human cell types. We previously shown that type I IFN also restricts *T.*
341 *gondii* growth in human THP-1 macrophages (3) and we now show that this restriction is
342 downstream of RNF213.
343 We observed that RNF213 was recruited to a proportion of parasite containing vacuoles
344 even in unstimulated cells, consistent with the fact that it is expressed at basal levels yet
345 induced by IFN-γ. Similarly, RNF213 has been shown to be recruited to vacuoles containing
346 intracellular *Salmonella* (42), *Listeria* (46), and *Chlamydia* lacking the effector GarD (47), and to
347 restrict their growth in the absence of IFN-γ stimulation. We observed a slight increase in the
348 growth of *T. gondii* in non-stimulated cells lacking RNF213; however, the major role for this
349 factor was in IFN-γ treated cells which completely lost growth inhibition in the absence of
350 RNF213. Notably, RNF213 was recruited early during infection and was associated with
351 ubiquitination of targets on the parasite containing vacuole. It was also present there before
352 autophagy marker LC3 and notably its presence on the vacuole did not rely on ATG5.
353 Moreover, the growth restriction imparted by IFN-γ treatment was largely independent of ATG5

354 and yet fully dependent on RNF213. Taken together, these finding suggest a model whereby
355 RNF213 is initially recruited to the parasite-containing vacuole where it ubiquitinates unknown
356 targets leading to growth restriction, followed by recruitment of a non-canonical ATG pathway,
357 which while not required for growth restriction may be important in downstream events.
358 The mechanism by which RNF213 is recruited to pathogen containing vacuoles remains
359 undefined, but the broad specificity of this pathway suggests that there may be some common
360 determinant recognized by the multiple domain structure of RNF213 that includes a dynein-like
361 core with 6 ATPase units and a multi-domain E3 module (48). Similarly, the targets of
362 ubiquitination on other pathogen-containing vacuoles remain undefined. Previous studies have
363 suggested LPS on cytoplasmically exposed *Salmonella* is targeted by ubiquitination (42),
364 although the exact chemical adduct remains to be defined. However, other pathogens including
365 intracellular *Listeria*, and various viruses that have been shown to be targeted by RNF213 (46),
366 lack LPS. The pathogens studied here also do not contain LPS, indicating that they must be
367 recognized by a different mechanism. The broad nature of organisms targeted by RNF213
368 favors a model in which RNF213 recognizes a host target, either protein or lipid, whose
369 modification leads to restricted pathogen growth. Future studies to elucidate this mechanism
370 may enable enhanced cell-autonomous immunity to clear intracellular pathogens without the
371 adverse effects of treatment with interferons.
372

373 **Acknowledgements**

374 We thank Dr. Wandy Beatty, Microbiology Imaging Facility, Washington University in St. Louis
375 for performing the electron microscopy studies. We also thank Jennifer Barks for cell culture
376 support, members of the Sibley lab for helpful comments, Robert Orchard for advice on the
377 CRISPR screens, and Felix Randow for communications prior to publication. This work was
378 presented prior to publication at the Woods Hole Immunoparasitology Meeting (April 10-13,
379 2022) and the 16th International Congress on Toxoplasmosis (May 22-26, 2022). Supported in
380 part by grants from the NIH (AI154048, AI118426).
381

382 **Author contributions**

383 Conceptualization: SKM, LDS; Data curation, SKM; Investigation; SKM, HPK, PC; Formal
384 Analysis, SKM, HPK, PC; Methodology: AB, JD; Project administration and supervision, JAP,
385 SD, LDS; Visualization SKM, HPK, PC; Writing, SKM, SD, JAP, LDS.
386

387 **Database submission**

388 RNASeq data have been submitted to GEO under the accession number GSE215771 and will
389 be made available to reviewers and released prior to publication.
390

391 ## Supplementary Materials

392

393 **Fig. S1A Validation of STAT1 knockout A549 line.**
394 **Fig. S1B Comparison of top hits for four primary CRISPR screens.**
395 **Fig. S2 Validation of IRF-1 and NF2 knockouts in A549 cells.**
396 **Fig. S3 Summary of NF2 dependent genes based on RNASeq.**
397 **Fig. S4 Validation of RNF213 knockouts in HFF and THP-1 cells.**
398 **Fig. S5 IFA staining of RNF213 and ubiquitination in CTG infected IFN-γ activated HFF**
399 **and THP-1 cells.**
400 **Table S1 Primers used for sgRNA cloning**
401 **Dataset 1 Results of four primary CRISPR screens.**
402 **Dataset 2 Results of pooled secondary CRISPR screens.**
403 **Dataset 3 Results of ISG targeted CRISPR screens.**
404

405 ## Materials and Methods

406 ### Reagents and antibodies

407 Rabbit polyclonal anti-RNF213 (#HPA003347), Tryptophan, puromycin, polybrene and phorbol
408 12-myristate 13-acetate (PMA) were obtained from Sigma-Aldrich (St. Louis, MO, USA). Human
409 IFN-γ, human TNF-α and human IFN-β were obtained from R&D systems (Minneapolis, MN,
410 USA). *T. gondii* parasites were stained with mouse mAb DG52 against the surface antigen
411 SAG1 (49) and GRA7 was detected using a rabbit polyclonal serum described previously (50).
412 Mouse monoclonal anti-polyubiquitin (FK2, # 04-0263) antibody was obtained from Millipore
413 Sigma Life Sciences. Rabbit mAb anti-IRF1 (D5E4, # 8478) and rabbit mAb anti-STAT1 (D1K9Y
414 #14994) were obtained from Cell Signaling Technologies. Rabbit polyclonal LC3 (# PM036) was
415 obtained from MBL International Corporation. Rabbit polyclonal anti-NF2 (ab217016) antibody
416 was obtained from Abcam. Mouse monoclonal anti-ATG5 (#66744-1-Ig) was obtained from
417 Proteintech Group, Inc. Secondary anti-IgGs conjugated to IRDye800 and IRDye700 were
418 obtained from Li-Cor Biosciences (Lincoln, NE, USA). Hoechst, goat anti-mouse IgG and goat
419 anti-rabbit IgG secondary antibodies conjugated to Alexa 488 or Alexa 594, were obtained from
420 Life technologies Corporations (Grand Island, NY, USA). Secondary anti-IgG conjugated to 18

421 nm gold particle in immuno-electron microscopy was obtained from Jackson ImmunoResearch
422 Laboratories, Inc., (West Grove, PA).
423

424 **Parasite and mammalian culture**

425 Type III CTG expressing GFP parasites were generated previously (34). Parasites were grown
426 as tachyzoites in human foreskin fibroblasts (HFF) obtained from the laboratory of Dr. John
427 Boothroyd, Stanford University, as described previously (9). Parasites were harvested shortly
428 after natural egress and purified by passage through 20 g needle and separated from host cell
429 debris using 3.0 micron polycarbonate filters (Whatman). HFFs, HEK-293T and A549 lung
430 epithelial carcinoma cells were maintained in DMEM with 10% v/v FBS at 5% CO_2 and 37 ^{0}C.
431 THP-1 human monocytic cells were maintained in RPMI with 10% v/v FBS at 5% CO_2 and 37
432 ^{0}C. THP-1 cells were first differentiated into macrophages with 50 nM PMA for 48 h. PMA was
433 washed off and cells were further incubated in their maintenance media for 24 h before use. All
434 strains and host cell lines were determined to be mycoplasma-negative using the e-Myco Plus
435 Kit (Intron Biotechnology).

436 **Lentiviral transduction of the Brunello library**

437 The Brunello library (# 73179) expressing 76,441 sgRNAs against 19,114 human genes + 1,000
438 non-targeting sgRNA controls in plentiCRISPRv2 was obtained from Addgene (51). The library
439 was electroporated into Endura electrocompetent cells (# 60242; Lucigen Bioresearch
440 Technologies) and plasmid was prepared from > 80 million bacterial colonies (>1,000X
441 representation). Briefly, twenty-five 60 mm tissue culture dishes, each containing 2.6 million
442 293T cells, were plated 24 h prior to transfection. A combination of 15 μg of plentiCRISPRv2
443 harboring the Brunello library, 5μg of pRSV-Rev (Addgene # 12253), 7 μg of pMD2.G (Addgene
444 # 12259), and 11 μg of pMDLg/pRRE (Addgene # 12251) were co-transfected per tissue culture
445 dish using Lipofectamine LTX reagent with PLUS reagent (Thermo Fisher Scientific) as per
446 manufacturer's instruction. The supernatant of 293T cells was collected 72 h after transfection
447 and filtered using 0.45 μm PES filter. A total of ten 150 mm tissue culture dishes, each
448 containing 10 million A549 cells, were seeded 24 h prior to virus transduction. The virus in the
449 supernatant was serially diluted and transduced into A549 cells using polybrene (8 ug/ml) to
450 achieve ~ 10% transduction efficiency. The media was changed 72 h after transduction and
451 cells were selected with 4 μg/ml of puromycin. In parallel, 800,000 A549 cells per well were
452 seeded in 6-well plates to calculate the coverage of transduced Brunello library. Transduced
453 coverage was calculated by measuring percent survival of virus transduced cells 72 h after

454 incubation with 4 μg/ml puromycin relative to untreated control. The cells were selected on 4
455 μg/ml puromycin for two weeks to select the transduced cells. The Brunello library transduced
456 A549 cells were passage 8 times before their use in the FACS based experiments. The library
457 transduced cells were always spilt at a minimum of 100X coverage or 7.5 million cells in new
458 T350 cm^2 tissue culture flasks for every passage until completion of the experiment.

459 **Cloning of secondary sgRNA CRISPR library**

460 Secondary screen: sgRNAs of genes that were significantly enriched (log2Fold Change > 1 and
461 $P < 0.05$) in T5 over uninfected control in 2 out of 4 replicates of the primary Brunello library
462 screens were selected to conduct a secondary screen. Ten sgRNAs per gene against 224
463 selected genes were designed using sgRNA designer at the Genetic Perturbation Platform
464 (GPP) web portal (https://portals.broadinstitute.org/gpp/public/analysis-tools/sgrna-design).
465 Additionally, 260 negative control sgRNAs were randomly selected from 1,000 negative control
466 sgRNAs in the Brunello library with 130 each corresponding to NO_SITE and
467 ONE_INTERGENIC_SITE negative controls. The oligonucleotide library was synthesized at
468 Genescript. Briefly, the 20 bp sgRNAs in the library were flanked by complementary sequences
469 in the plentiCRISPRv2 vector with CTTGTGGAAAGGACGAAACACCG oligonucleotide at the 5'
470 end and GTTTTAGAGCTAGAAATAGCAAGTTAAAATAAGGC at the 3' end. The library was
471 PCR amplified and Gibson cloned (52) into BsmBI digested plentiCRISPRv2. Assembled
472 plasmid was dialyzed on a Type-VS Millipore membrane (MF type, VS filter, mean pore size =
473 0.025 μm, Millipore, Inc. #VSWP 02500) and electroporated into Endura electrocompetent cells.
474 A549 cells were transduced with the secondary pool library at > 100X coverage, as described
475 above, and selected with 4 μg/ml puromycin for two weeks. The secondary library transduced
476 cells were passage 8 times before their use in the FACS based experiments and were always
477 spilt at a minimum of 100X coverage for every passage until completion of the experiment.
478

479 **Cloning of the Interferon Stimulated Gene (ISG) sgRNA library**

480 Genes that are significantly induced in A549 cells upon IFN-γ stimulation (34) were selected for
481 sgRNA design. Ten sgRNA per gene were designed for 352 ISGs using the GPP web portal. A
482 total of 480 negative control sgRNAs were randomly selected from 1,000 negative control
483 sgRNAs from the Brunello library with 240 each corresponding to NO_SITE and
484 ONE_INTERGENIC_SITE negative controls. The oligonucleotide library was synthesized at
485 Genescript. The 20 bp sgRNAs in this library were flanked by BsmBI recognition sites along with
486 overhang sequence for ligation with BsmBI digested plentiCRISPRv2. The 79 oligonucleotide

487 library consists of 20 bp sgRNA sequences flanked with 5'
488 GCACTTGCTCGTACGACGCGTCTCACACCG sequence and 3'
489 GTTTCGAGACGTTAAGGTGCCGGGCCCAC sequence. The library was PCR amplified,
490 digested with BsmBI, and ligated into plentiCRISPRv2 using NEB Golden Gate Assembly Kit
491 (BsmBI-v2) (New England Biolabs Inc. # E1602S). The ligation reaction was dialyzed on a
492 Type-VS Millipore membrane and electroporated into Endura electrocompetent cells. A549 cells
493 were transduced with the ISG library at > 100X coverage, as described above and selected on 4
494 μg/ml puromycin for two weeks. The ISG library transduced cells were passage 8 times before
495 their use in the FACS based experiments and were always spilt at a minimum of 100X coverage
496 for every passage until completion of the experiment.

497 **Flow cytometry and cell sorting**

498 Wild type and STAT1 knockout (STAT1 KO) A549 cells were cultured ± 100 U/ml IFN-γ for 24 h
499 prior followed by washing with complete media. The cells were infected with CTG expressing
500 GFP (CTG-GFP) at MOI 0.5 and cultured for 40 h. Cells were washed, trypsinized, and fixed
501 with 4% paraformaldehyde followed by analysis on Sony SH800S cell sorter. Single cells were
502 gated and GFP fluorescence was used to monitor intracellular growth of CTG-GFP. FACS-
503 based CRISPR screens were executed by pre-activating 30-50 million library transduced A549
504 cells with 100 U/ml of IFN-γ for 24 h. The cells were washed and infected with CTG-GFP at MOI
505 0.5 and incubated for 40 h. Cells were washed, trypsinized, and filtered (40 μm) prior to sorting.
506 Single cells were gated and top 5% of events (T5) based on GFP fluorescence intensity were
507 sorted. Genomic DNA was isolated from the top 5% CTG-GFP infected cells and uninfected
508 cells for each of 4 biological replicates for each library. Uninfected control cells for each
509 replicate were passage matched with the sorted T5 population.

510 **Genomic DNA isolation and next generation sequencing**

511 Genomic DNA was isolated using Qiagen DNeasy kit as per manufacturer's instructions. PCR
512 was done using Ex Taq in a 100 μl reaction with the maximum of 10 μg of template per reaction
513 (36). The amplicons for next generation sequencing were generated using a 2-step PCR
514 amplification of integrated sgRNAs. Briefly, genomic DNA isolated from different samples was
515 used as template for PCR1 using forward 5'
516 TCGTCGGCAGCGTCAGATGTGTATAAGAGACAGGGCTTTATATATCTTGTGGAAAGGACGA
517 AACACC 3' and reverse 5'
518 GTCTCGTGGGCTCGGAGATGTGTATAAGAGACAGCCAATTCCCACTCCTTTCAAGACCT 3'
519 primers with PCR cycling conditions of 30s 95 ^{0}C, 30s 53 ^{0}C, 30s 72 ^{0}C for 18-24 cycles. PCR2

520 was performed using 5 µl of PCR1 as template using forward 5'
521 AATGATACGGCGACCACCGAGATCTACAC-10bp barcode-TCGTCGGCAGCGTC 3' and
522 reverse 5' CAAGCAGAAGACGGCATACGAGAT-10bp barcode-GTCTCGTGGGCTCGG 3'
523 primers with PCR cycling conditions of 30s 95 ^{0}C, 30s 54 ^{0}C, 30s 72 ^{0}C for 24 cycles. PCR2
524 amplicons were uniquely dual indexed with 10 bp Illumina-compatible barcodes for each
525 sample. The samples within each screen were pooled and submitted to the Genome
526 Technology Access Center, Washington University School of Medicine in St. Louis for next
527 generation sequencing on an Illumina NovaSeq-6000 with at least 100x coverage of 150 bp
528 paired end reads. Basecalls and demultiplexing were performed with Illumina's bcl2fastq2
529 software. The forward reads were analyzed using MAGeCK as described previously (53).
530 Briefly, read counts for the sgRNAs sequences were normalized and counted using the count
531 function followed by comparison between the T5 population and uninfected control using the
532 test function. The data was analyzed in R using the MAGeCKFlute package (54). Log_2Fold
533 change of sgRNAs in T5 population relative to uninfected control was plotted against -Log_{10}FDR
534 (False Discovery Rate).

535 **RNA Sequencing**

536 Cells were seeded in a 6-well plate overnight and then treated ± IFN-γ (100 U/ml) for 24 h. The
537 cells were lysed, and total RNA was extracted using QIAGEN RNeasy Mini Kit as per
538 manufacturer's instructions. The RNA samples were prepared from 3 independent biological
539 replicates and submitted to the Genome Technology Access Center, Washington University
540 School of Medicine in St. Louis, for next-generation mRNA sequencing. Library preparation was
541 performed using ~ 1ug of total RNA processed using RiboErase kits to remove ribosomal RNA
542 (Kapa Biosystems). mRNA was then fragmented in reverse transcriptase buffer and heating to
543 94 ^{0}C for 8 min. mRNA was reverse transcribed to yield cDNA using SuperScript III RT enzyme
544 (Life Technologies, per manufacturer's instructions) using random hexamers. A second strand
545 reaction was performed to yield ds-cDNA that was blunt ended, extended by adding an A base
546 to the 3' ends, and followed by ligation of Illumina sequencing adapters. Ligated fragments were
547 then amplified for 12-15 cycles using primers incorporating unique dual index tags. Fragments
548 were sequenced on an Illumina NovaSeq-6000 to generate paired end reads extending 150
549 bases. Basecalls and demultiplexing were performed with Illumina's bcl2fastq2 software. A total
550 of 1,046,709,676 reads from 18 samples were generated and the fastq files were imported into
551 CLC Genomics Workbench version 21.0.5 (QIAGEN Bioinformatics, Inc.). The reads were
552 aligned to Homo sapiens hg38 reference genome (downloaded from Ensembl via the CLC
553 Genomics Workbench) that covered 60,676 genes and 204,381 transcripts in total. The

554 expression data from the CLC Genomics Workbench were imported into R to generate heat
555 map of differentially expressed genes and compare RPKM values of ISGs across samples.

556 **CRISPR-Cas9 mediated gene deletions**

557 sgRNAs were designed using the GPP web portal and 20 bp sgRNAs were synthesized as
558 primer pairs (**Table S1.xlsx**) with overhanging BsmBI sites and ligated to BsmBI digested
559 plentiCRISPRv2. sgRNAs cloned into the plentiCRIPSRv2 plasmid was packaged into
560 lentiviruses by co-transfecting into 293T cells in equimolar ratio with pRSV-Rev, pMD2.G and
561 pMDLg/pRRE. The supernatant was collected 72 h post transfection and the virus was filtered
562 through 0.45 μm PES filter. The virus containing supernatant was titrated and was transduced
563 into different cell lines at 10% transduction efficiency for 72 h. The cells were washed and
564 incubated with puromycin (4 μg/ml for A549, 2 μg/ml for THP-1 and 1 μg/ml HFFs) for 10 days
565 to select stably transduced cells. Single cell knockouts of IRF-1, NF2, and RNF213 were
566 isolated by FACS sorting single cell per well. STAT1 KO A549 cells, ATG5 KO A549 cells and
567 RNF213 KO HFF cells were maintained at the population level. Gene deletion of host factors
568 was confirmed by western blot and Sanger sequencing of the editing site.

569 **Vacuolar size growth assay**

570 Parasite growth was monitored using a vacuolar size assay that was performed as described
571 previously (9). Briefly, host cells were seeded in 96-well μCLEAR black plates (Greiner Bio-One
572 International GmbH) for 24 h before use. For THP-1, the cells were first differentiated with 50
573 nM PMA for 48 h before addition of 100 U/ml of IFN-γ or 100 U/ml IFN-β with 10 ng/ml of TNF-α
574 for 24 h prior to infection. The cells were cultured ± 100 U/ml of IFN-γ for 24 h and then washed
575 with warm PBS. The cells were infected with parasites at MOI 0.5 for 2 h, washed with warm
576 PBS to remove extracellular parasites, and returned to culture in complete medium for different
577 intervals. Cells were fixed with 4% paraformaldehyde, permeabilized using 0.02% saponin in
578 5% FBS (Fetal bovine serum) +5% NGS (Normal goat serum) and stained to detect parasites
579 (anti-SAG1) and the parasitophorous vacuole (anti-GRA7), followed by Alexa-fluor conjugated
580 secondary antibodies, and Hoechst (100 ng/ml) to stain the nuclei. Images were acquired at a
581 magnification of 20x on a Cytation3 cell imaging multi-mode plate-based imager (BioTek). The
582 size of parasitophorous vacuole-harboring parasites (SAG1-positive GRA7 vacuoles) was
583 determined using CellProfiler 2.1.1. Data from at least 50 fields per sample in each of three
584 independent experiments were used to calculate the vacuolar size of parasites in different host
585 cells.

586 **ISRE promoter assay**

587 Cells per well were seeded at a density of 25,000 per 96-well plate and cultured overnight. The
588 cells were co-transfected with 50 ng of plasmid expressing ISRE reporter (9) and 50 ng of
589 pCMV-Red Firefly Luc Vector (Thermo Fisher Scientific # 16156) using lipofectamine LTX
590 (Thermo Fisher Scientific) according to the manufacturer's instructions. The cells were washed
591 with warm DMEM (with 10% v/v FBS) and cultured ± 100 U/ml human IFN-β for another 24 h.
592 Gaussia luciferase activity was measured in the supernatant using the Pierce Gaussia
593 luciferase glow assay kit (Thermo Fisher Scientific # 16160). Firefly luciferase activity was
594 measured in the cell lysates after removing the supernatant and washing the cells with warm
595 PBS using the Pierce Firefly luciferase glow assay kit (Thermo Fisher Scientific # 16176).
596 Luminescence was measured in Cytation3 multi-mode plate reader. ISRE promoter activity was
597 calculated by normalizing gaussian luminescence to firefly luminescence for each sample.

598 **Immunofluorescence staining**

599 Cells were seeded onto 12 mm coverslips in a 24-well overnight and then treated ± 100 U/ml
600 human IFN-γ for 24 h. The cells were washed with warm PBS and infected with CTG-GFP
601 parasites at MOI 3 for 6h. The cells were washed to remove extracellular parasites and fixed
602 with 4% paraformaldehyde for 20 min at room temperature. Cells were permeabilized and
603 blocked in using 5% FBS and 5% normal goat serum with 0.02% saponin in PBS for 30 min.
604 Cell were stained with FK2 (1:2,000; anti-mono- and poly-ubiquitinated proteins) and anti-
605 RNF213 (1:2,000) and/or anti-LC3 (1:2,000) in 1% FBS with 0.02% saponin in PBS for 90 min.
606 Cells were washed three times with PBS and incubated with Alexa-fluor conjugated secondary
607 antibodies (1:4,000) and Hoechst stain (100 ng/ml) to stain nuclei (Life Technologies) for 30
608 min. Cells were then washed three times with PBS followed by mounting in ProLong gold
609 antifade mountant (Thermo Fisher Scientific). Images were acquired using a 63x oil Plan-
610 Apochromat lens (N.A. 1.4) on an Axioskop2 MOT Plus Wide Field Fluorescence Microscope
611 (Carl Zeiss) or using a LSM880 confocal laser scanning microscope (Carl Zeiss) in the
612 Microbiology Imaging Facility, Washington University in St. Louis.

613 **Western blotting**

614 Cells were lysed using CellLytic M (Sigma) with complete mini protease inhibitor cocktail
615 (Roche). The lysates were centrifuged at 6,000 *g* for 10 min at room temperature to pellet
616 nuclear debris. Total protein was measured using BCA (bicinchoninic acid) protein assay kit
617 (Thermo Fisher Scientific). Samples were boiled at 95 ^{0}C for 15 min in Laemmli buffer
618 containing 100 mM dithiothreitol (DTT), separated by SDS-PAGE and transferred onto
619 nitrocellulose membranes. Membranes were blocked in a 1:1 mixture of Odyssey blocking

620 buffer (OBB; Li-Cor Biosciences) and PBS overnight at 4°C. Membranes were incubated with
621 primary antibodies (1:4,000) for 2 h at room temperature in a 1:1 mixture of Odyssey blocking
622 buffer and PBS with 0.1% Tween 20 (PBST). Blots were washed thrice with PBST and
623 incubated with anti-mouse IgG IR800 and anti-mouse IgG IR700 at 1:15,000 for 2 h at RT in a
624 1:1 mixture of Odyssey blocking buffer and PBST. The blot was washed thrice with PBST
625 followed by infrared imaging on a Li-Cor Odyssey imaging system.

626 ***M. tuberculosis* strains and infections**

627 *M. tuberculosis* (Mtb) was grown at 37 °C to log phase in Middlebrook 7H9 broth (BD
628 Biosciences) supplemented with 0.05% Tyloxapol, BD BBL Middlebrook OADC Enrichment (BD
629 Biosciences), and 0.2% (v/v) glycerol. H37Rv (the wild type strain) and H37Rv-GFP (GFP-
630 expressing fluorescent strain) were originally provided by William Jacobs Jr. (Albert Einstein
631 College of Medicine). H37Rv-GFP was maintained in broth containing 25 µg/mL kanamycin. For
632 *in vitro* infection assays, a log phase culture of *M. tuberculosis* was used to prepare single-cell
633 suspensions using the slow centrifugation method. Bacteria were pelleted, resuspended in cell
634 culture medium, and centrifuged at 800 rpm for 8 minutes. The supernatant was collected, and
635 the number of bacilli was estimated by measuring absorbance at 600 nm. This step was
636 repeated until a constant absorbance value was obtained. For *in vitro* infection, cells were
637 seeded in 96 well plates overnight followed by culture ± human IFN-γ (100 units/mL) for 24 h.
638 Cells were washed and infected with Mtb at MOI 0.5. After 4 hours, cells were washed three
639 times with warm DMEM to remove extracellular bacteria, and then resuspended in culture
640 medium. To estimate intracellular bacterial growth, infected cells were lysed in 0.06% SDS
641 solution at the indicated time points, and serial dilutions of the lysates were plated on 7H11 agar
642 plates (BD Biosciences, catalog no. 283810) containing BD BBL Middlebrook OADC
643 Enrichment (BD Biosciences, catalog no. 212351) and glycerol. Colony forming units (CFU)
644 were calculated 14-21 days later. For immunofluorescence assays, H37Rv-GFP infected cells
645 were fixed at 8 hpi with 4% paraformaldehyde for one hour, permeabilized and blocked in PBS
646 with 0.05% Triton X-100 and 3% BSA and stained with FK2 (1:2,000) and anti-RNF213
647 (1:2,000) overnight at 4 ^{0}C. Staining with Alexa fluorophore-conjugated secondary antibody
648 (Molecular Probes) was done for 2 h at room temperature. Following this, the samples were
649 washed with 0.1% Tween 20/PBS and mounted using Prolong Gold antifade (Thermo Fisher
650 Scientific, # P36930). Images were captured using a Nikon Eclipse Ti confocal microscope
651 (Nikon Instruments Inc.) equipped with a 60X apochromat oil-objective lens and analyzed using
652 NIS-Elements version 4.40 (Nikon).

653 **Vesicular Stomatitis virus (VSV) culture and infections**

654 Recombinant vesicular stomatitis virus (VSV) expressing enhanced green fluorescent protein
655 (eGFP; VSV-GFP) (55) was propagated as previously described (56) in either African Green
656 Monkey kidney Vero E6 (CRL-1586, ATCC) or MA104 cells (CRL-2378.1). Vero E6 cells and
657 MA104 cells were cultured in complete DMEM media and complete M199 media, respectively.
658 Viral titers were determined by standard plaque assays. Cells were seeded at 10,000 per well in
659 24-well plates and cultured overnight followed by culture in ± 100 U/ml human IFN-β for 24 h.
660 The cells were washed and infected with VSV-GFP at MOI 1 for 24 h, as described previously
661 (57). GFP intensity was determined by scanning with an Amersham Typhoon 5 (GE) and
662 images quantified by ImageJ. The number of total intensities subtracted from background was
663 computed for each treatment and $\log_{10}$ transformed.

664 **Immuno-electron microscopy**

665 Wild type A549 cells were pre-activated with IFN-γ (100 U/ml) 24 h prior to infection with CTG
666 for 6h. The cells were trypsinized and fixed in 4% paraformaldehyde/0.01% glutaraldehyde
667 (Polysciences Inc., Warrington, PA) in 100 mM PIPES/0.5 mM $MgCl_2$, pH 7.2 for 1 h at 4
668 °C. Samples were then embedded in 10% gelatin and infiltrated overnight with 2.3 M
669 sucrose/20% polyvinyl pyrrolidone in PIPES/$MgCl_2$ at 4 °C. Samples were trimmed, frozen in
670 liquid nitrogen, and sectioned with a Leica Ultracut UCT7 cryo-ultramicrotome (Leica
671 Microsystems Inc., Bannockburn, IL). Ultrathin sections of 50 nm were blocked with 5% FBS
672 (fetal bovine serum)/5% NGS (normal goat serum) for 30 min and subsequently incubated with
673 rabbit anti-RNF213 antibody for 1 h at room temperature. Following washes in block buffer,
674 sections were incubated with secondary anti-rabbit IgG antibody conjugated to 18 nm colloidal
675 gold (Jackson ImmunoResearch Laboratories, Inc., West Grove, PA) for 1 h. Sections were
676 stained with 0.3% uranyl acetate/2% methyl cellulose and viewed by transmission electron
677 microscopy. All labeling experiments were conducted in parallel with controls omitting the
678 primary antibody.

679 **Transmission electron microscopy**

680 Wild type A549 cells were pre-activated with IFN-γ (100 U/ml) 24 h prior to infection with CTG
681 for 6h. The cells were trypsinized and fixed freshly prepared mixture of 1% glutaraldehyde
682 (Polysciences Inc, Warrington, PA) and 1% osmium tetroxide (Polysciences Inc.) in 50 mM
683 phosphate buffer at 4ºC for 30 min. Samples were then rinsed extensively in cold dH_20 prior to
684 en bloc staining with 1% aqueous uranyl acetate (Ted Pella Inc., Redding, CA) at 4 ºC for 3
685 h. Following several rinses in dH_20, samples were dehydrated in a graded series of ethanol and

686 embedded in Eponate 12 resin (Ted Pella Inc.). Sections of 95 nm were cut with a Leica
687 Ultracut UCT ultramicrotome (Leica Microsystems Inc., Bannockburn, IL), stained with uranyl
688 acetate and lead citrate, and viewed on a JEOL 1200 EX transmission electron microscope
689 (JEOL USA Inc., Peabody, MA) equipped with an AMT 8 megapixel digital camera and AMT
690 Image Capture Engine V602 software (Advanced Microscopy Techniques, Woburn, MA).

691 **Statistical analysis**

692 All experiments were performed in 3 independent biological repeats unless mentioned
693 otherwise. Statistical analysis for each experiment was performed on the combined data in
694 PRISM. Significance values and tests performed are included in the figure legends.

695

696 ## References

697 1. Sibley LD. 2011. Invasion and intracellular survival by protozoan parasites.
698 Immunological Reviews 240:72-91.
699 2. Blader IJ, Coleman BI, Chen CT, Gubbels MJ. 2015. Lytic Cycle of Toxoplasma gondii: 15
700 Years Later. Annu Rev Microbiol 69:463-85.
701 3. Clough B, Frickel EM. 2017. The Toxoplasma Parasitophorous Vacuole: An Evolving Host-
702 Parasite Frontier. Trends Parasitol 33:473-488.
703 4. Khan IA, Moretto M. 2022. Immune responses to Toxoplasma gondii. Curr Opin
704 Immunol 77:102226.
705 5. Frickel EM, Hunter CA. 2021. Lessons from Toxoplasma: Host responses that mediate
706 parasite control and the microbial effectors that subvert them. J Exp Med 218.
707 6. Yap GS, Sher A. 1999. Effector cells of both nonhemopoietic and hemopoietic origin are
708 required for interferon (IFN)-gamma- and tumor necrosis factor (TNF)-alpha- dependent
709 host resistance to the intracellular pathogen, *Toxoplasma gondii*. J Exp Med 189:1083-
710 1091.
711 7. Suzuki Y, Orellana MA, Schreiber RD, Remington JS. 1988. Interferon-g: the major
712 mediator of resistance against *Toxoplasma gondii*. Science 240:516-518.
713 8. Han SJ, Melichar HJ, Coombes JL, Chan SW, Koshy AA, Boothroyd JC, Barton GM, Robey
714 EA. 2014. Internalization and TLR-dependent type I interferon production by monocytes
715 in response to Toxoplasma gondii. Immunol Cell Biol 92:872-81.
716 9. Matta SK, Olias P, Huang Z, Wang Q, Park E, Yokoyama WM, Sibley LD. 2019.
717 *Toxoplasma gondii* effector TgIST blocks type I interferon signaling to promote infection.
718 Proc Natl Acad Sci U S A 116:17480-17491.
719 10. Mostafavi S, Yoshida H, Moodley D, LeBoite H, Rothamel K, Raj T, Ye CJ, Chevrier N,
720 Zhang SY, Feng T, Lee M, Casanova JL, Clark JD, Hegen M, Telliez JB, Hacohen N, De Jager
721 PL, Regev A, Mathis D, Benoist C, Immunological Genome Project C. 2016. Parsing the
722 Interferon Transcriptional Network and Its Disease Associations. Cell 164:564-78.
723 11. Rusinova I, Forster S, Yu S, Kannan A, Masse M, Cumming H, Chapman R, Hertzog PJ.
724 2013. Interferome v2.0: an updated database of annotated interferon-regulated genes.
725 Nucleic Acids Res 41:D1040-6.

726 12. Howard JC, Hunn JP, Steinfeldt T. 2011. The IRG protein-based resistance mechanism in
727 mice and its relation to virulence in *Toxoplasma gondii*. Curr Opin Microbiol 14:414-21.
728 13. Gazzinelli RT, Mendonca-Neto R, Lilue J, Howard J, Sher A. 2014. Innate resistance
729 against Toxoplasma gondii: an evolutionary tale of mice, cats, and men. Cell Host
730 Microbe 15:132-8.
731 14. MacMicking JD. 2012. Interferon-inducible effector mechanisms in cell-autonomous
732 immunity. Nat Rev Immunol 12:367-82.
733 15. Zhao Z, Fux B, Goodwin M, Dunay IR, Strong D, Miller BC, Cadwell K, Delgado MA,
734 Ponpuak M, Green KG, Schmidt RE, Mizushima N, Deretic V, Sibley LD, Virgin HW. 2008.
735 Autophagosome-independent essential function for the autophagy protein Atg5 in
736 cellular immunity to intracellular pathogens. Cell Host Microbe 4:458-469.
737 16. Ohshima J, Lee Y, Sasai M, Saitoh T, Su Ma J, Kamiyama N, Matsuura Y, Pann-Ghill S,
738 Hayashi M, Ebisu S, Takeda K, Akira S, Yamamoto M. 2014. Role of mouse and human
739 autophagy proteins in IFN-gamma-induced cell-autonomous responses against
740 *Toxoplasma gondii*. J Immunol 192:3328-35.
741 17. Choi J, Park S, Biering S, Selleck EM, Liu C, Zhang X, Fujita N, Saitoh T, Akira S, Yoshimori
742 T, Sibley LD, Hwang S, Virgin HW. 2014. The parasitophorous vacuole membrane of
743 *Toxoplasma gondii* is targeted for disruption by ubiquitin-like conugation systems of
744 autophagy. Immunity in press.
745 18. Hoffmann C, Ernst M, Meyer P, Wolf E, Rosenkranz T, Plettenberg A, Stoehr A, Horst HA,
746 Marienfeld K, Lange C. 2007. Evolving characteristics of toxoplasmosis in patients
747 infected with human immunodeficiency virus-1: clinical course and Toxoplasma gondii-
748 specific immune responses. Clin Microbiol Infect 13:510-5.
749 19. Meira CS, Pereira-Chioccola VL, Vidal JE, de Mattos CC, Motoie G, Costa-Silva TA, Gava R,
750 Frederico FB, de Mattos LC, Toxoplasma G. 2014. Cerebral and ocular toxoplasmosis
751 related with IFN-gamma, TNF-alpha, and IL-10 levels. Front Microbiol 5:492.
752 20. Murray HW, Granger AM, Teitelbaum RF. 1991. Gamma interferon-activated human
753 macrophages and *Toxoplasma gondii*, *Chalmydia psittaci*, and *Leishmania donovani*:
754 antimicrobial role of limiting intracellular iron. Infection and Immunity 59:4684-4686.
755 21. Nathan CF, Murray HW, Weibe ME, Rubin BY. 1983. Indentification of interferon gamma
756 as the lymphokine that activates human macrophage oxidative metabolism and
757 antimicrobial activity. J Exp Med 158:670-689.
758 22. Orellana MA, Suzuki Y, Araujo F, Remington JS. 1991. Role of beta interferon in
759 resistance to Toxoplasma gondii infection. Infect Immun 59:3287-90.
760 23. Schmitz JL, Carlin JM, Borden EC, Byrne GI. 1989. Beta interferon inhibits Toxoplasma
761 gondii growth in human monocyte-derived macrophages. Infect Immun 57:3254-6.
762 24. Matta SK, Rinkenberger N, Dunay IR, Sibley LD. 2021. Toxoplasma gondii infection and
763 its implications within the central nervous system. Nat Rev Microbiol 19:467-480.
764 25. Pfefferkorn ER. 1984. Interferon-gamma blocks the growth of *Toxoplasma gondii* in
765 human fibroblasts by inducing the host to degrade tryptophan. Proc Natl Acad Sci (USA)
766 81:908-912.
767 26. Daubener W, Spors B, Hucke C, Adam R, Stins M, Kim KS, Schroten H. 2001. Restriction
768 of Toxoplasma gondii growth in human brain microvascular endothelial cells by
769 activation of indoleamine 2,3-dioxygenase. Infect Immun 69:6527-31.

770 27. Selleck EM, Orchard RC, Lassen KG, Beatty WL, Xavier RJ, Levine B, Virgin HW, Sibley LD.
771 2015. A noncanonical autophagy pathway restricts *Toxoplasma gondii* growth in a
772 strain-specific manner in IFN-gamma-activated human cells. MBio 6:e01157-15.
773 28. Bhushan J, Radke JB, Perng YC, McAllaster M, Lenschow DJ, Virgin HW, Sibley LD. 2020.
774 ISG15 Connects Autophagy and IFN-gamma-Dependent Control of Toxoplasma gondii
775 Infection in Human Cells. mBio 11.
776 29. Clough B, Wright JD, Pereira PM, Hirst EM, Johnston AC, Henriques R, Frickel EM. 2016.
777 K63-Linked Ubiquitination Targets Toxoplasma gondii for Endo-lysosomal Destruction in
778 IFNgamma-Stimulated Human Cells. PLoS Pathog 12:e1006027.
779 30. Hernandez D, Walsh S, Saavedra Sanchez L, Dickinson MS, Coers J. 2022. Interferon-
780 Inducible E3 Ligase RNF213 Facilitates Host-Protective Linear and K63-Linked
781 Ubiquitylation of Toxoplasma gondii Parasitophorous Vacuoles. mBio
782 doi:10.1128/mbio.01888-22:e0188822.
783 31. Johnston AC, Piro A, Clough B, Siew M, Virreira Winter S, Coers J, Frickel EM. 2016.
784 Human GBP1 does not localize to pathogen vacuoles but restricts Toxoplasma gondii.
785 Cell Microbiol 18:1056-64.
786 32. Fisch D, Bando H, Clough B, Hornung V, Yamamoto M, Shenoy AR, Frickel EM. 2019.
787 Human GBP1 is a microbe-specific gatekeeper of macrophage apoptosis and pyroptosis.
788 EMBO J 38:e100926.
789 33. Fisch D, Clough B, Khan R, Healy L, Frickel EM. 2022. Toxoplasma-proximal and distal
790 control by GBPs in human macrophages. Pathog Dis 79.
791 34. Rinkenberger N, Abrams ME, Matta SK, Schoggins JW, Alto NM, Sibley LD. 2021.
792 Overexpression screen of interferon-stimulated genes identifies RARRES3 as a restrictor
793 of Toxoplasma gondii infection. Elife 10.
794 35. Fentress SJ, Behnke MS, Dunay IR, Mashayekhi M, Rommereim LM, Fox BA, Bzik DJ,
795 Taylor GA, Turk BE, Lichti CF, Townsend RR, Qiu W, Hui R, Beatty WL, Sibley LD. 2010.
796 Phosphorylation of immunity-related GTPases by a Toxoplasma gondii-secreted kinase
797 promotes macrophage survival and virulence. Cell Host Microbe 8:484-95.
798 36. Doench JG, Fusi N, Sullender M, Hegde M, Vaimberg EW, Donovan KF, Smith I, Tothova
799 Z, Wilen C, Orchard R, Virgin HW, Listgarten J, Root DE. 2016. Optimized sgRNA design to
800 maximize activity and minimize off-target effects of CRISPR-Cas9. Nat Biotechnol
801 34:184-191.
802 37. Li W, You L, Cooper J, Schiavon G, Pepe-Caprio A, Zhou L, Ishii R, Giovannini M,
803 Hanemann CO, Long SB, Erdjument-Bromage H, Zhou P, Tempst P, Giancotti FG. 2010.
804 Merlin/NF2 suppresses tumorigenesis by inhibiting the E3 ubiquitin ligase CRL4(DCAF1)
805 in the nucleus. Cell 140:477-90.
806 38. Doench JG. 2018. Am I ready for CRISPR? A user's guide to genetic screens. Nat Rev
807 Genet 19:67-80.
808 39. Feng H, Zhang YB, Gui JF, Lemon SM, Yamane D. 2021. Interferon regulatory factor 1
809 (IRF1) and anti-pathogen innate immune responses. PLoS Pathog 17:e1009220.
810 40. James MF, Han S, Polizzano C, Plotkin SR, Manning BD, Stemmer-Rachamimov AO,
811 Gusella JF, Ramesh V. 2009. NF2/merlin is a novel negative regulator of mTOR complex
812 1, and activation of mTORC1 is associated with meningioma and schwannoma growth.
813 Mol Cell Biol 29:4250-61.

814 41. White SM, Avantaggiati ML, Nemazanyy I, Di Poto C, Yang Y, Pende M, Gibney GT,
815 Ressom HW, Field J, Atkins MB, Yi C. 2019. YAP/TAZ Inhibition Induces Metabolic and
816 Signaling Rewiring Resulting in Targetable Vulnerabilities in NF2-Deficient Tumor Cells.
817 Dev Cell 49:425-443 e9.
818 42. Otten EG, Werner E, Crespillo-Casado A, Boyle KB, Dharamdasani V, Pathe C, Santhanam
819 B, Randow F. 2021. Ubiquitylation of lipopolysaccharide by RNF213 during bacterial
820 infection. Nature 594:111-116.
821 43. Houzelstein D, Simon-Chazottes D, Batista L, Tokuda S, Langa Vives F, Flamand M,
822 Montagutelli X, Panthier JJ. 2021. The ring finger protein 213 gene (Rnf213) contributes
823 to Rift Valley fever resistance in mice. Mamm Genome 32:30-37.
824 44. Taniguchi T, Ogasawara K, Takaoka A, Tanaka N. 2001. IRF family of transcription factors
825 as regulators of host defense. Annu Rev Immunol 19:623-55.
826 45. O'Connell BC, Harper JW. 2007. Ubiquitin proteasome system (UPS): what can
827 chromatin do for you? Curr Opin Cell Biol 19:206-14.
828 46. Thery F, Martina L, Asselman C, Zhang Y, Vessely M, Repo H, Sedeyn K, Moschonas GD,
829 Bredow C, Teo QW, Zhang J, Leandro K, Eggermont D, De Sutter D, Boucher K,
830 Hochepied T, Festjens N, Callewaert N, Saelens X, Dermaut B, Knobeloch KP, Beling A,
831 Sanyal S, Radoshevich L, Eyckerman S, Impens F. 2021. Ring finger protein 213
832 assembles into a sensor for ISGylated proteins with antimicrobial activity. Nat Commun
833 12:5772.
834 47. Walsh SC, Reitano JR, Dickinson MS, Kutsch M, Hernandez D, Barnes AB, Schott BH,
835 Wang L, Ko DC, Kim SY, Valdivia RH, Bastidas RJ, Coers J. 2022. The bacterial effector
836 GarD shields Chlamydia trachomatis inclusions from RNF213-mediated ubiquitylation
837 and destruction. Cell Host Microbe doi:10.1016/j.chom.2022.08.008.
838 48. Ahel J, Lehner A, Vogel A, Schleiffer A, Meinhart A, Haselbach D, Clausen T. 2020.
839 Moyamoya disease factor RNF213 is a giant E3 ligase with a dynein-like core and a
840 distinct ubiquitin-transfer mechanism. Elife 9.
841 49. Burg JL, Perlman D, Kasper LH, Ware PL, Boothroyd JC. 1988. Molecular analysis of the
842 gene encoding the major surface antigen of *Toxoplasma gondii*. J Immunol 141:3584-
843 3591.
844 50. Alaganan A, Fentress SJ, Tang K, Wang Q, Sibley LD. 2013. Toxoplasma GRA7 effector
845 increases turnover of immunity-related GTPases and contributes to acute virulence in
846 the mouse. Proc Natl Acad Sci (USA) 111:1126-1131.
847 51. Sanjana NE, Shalem O, Zhang F. 2014. Improved vectors and genome-wide libraries for
848 CRISPR screening. Nat Methods 11:783-784.
849 52. Gibson DG. 2011. Enzymatic assembly of overlapping DNA fragments. Methods Enzymol
850 498:349-61.
851 53. Li W, Xu H, Xiao T, Cong L, Love MI, Zhang F, Irizarry RA, Liu JS, Brown M, Liu XS. 2014.
852 MAGeCK enables robust identification of essential genes from genome-scale
853 CRISPR/Cas9 knockout screens. Genome Biol 15:554.
854 54. Wang B, Wang M, Zhang W, Xiao T, Chen CH, Wu A, Wu F, Traugh N, Wang X, Li Z, Mei S,
855 Cui Y, Shi S, Lipp JJ, Hinterndorfer M, Zuber J, Brown M, Li W, Liu XS. 2019. Integrative
856 analysis of pooled CRISPR genetic screens using MAGeCKFlute. Nat Protoc 14:756-780.

857 55. Cherry S, Doukas T, Armknecht S, Whelan S, Wang H, Sarnow P, Perrimon N. 2005.
858 Genome-wide RNAi screen reveals a specific sensitivity of IRES-containing RNA viruses to
859 host translation inhibition. Genes Dev 19:445-52.
860 56. Li B, Ding S, Feng N, Mooney N, Ooi YS, Ren L, Diep J, Kelly MR, Yasukawa LL, Patton JT,
861 Yamazaki H, Shirao T, Jackson PK, Greenberg HB. 2017. Drebrin restricts rotavirus entry
862 by inhibiting dynamin-mediated endocytosis. Proc Natl Acad Sci U S A 114:E3642-E3651.
863 57. Ding S, Zhu S, Ren L, Feng N, Song Y, Ge X, Li B, Flavell RA, Greenberg HB. 2018.
864 Rotavirus VP3 targets MAVS for degradation to inhibit type III interferon expression in
865 intestinal epithelial cells. Elife 7.
866
867

868 **Figures Legends**

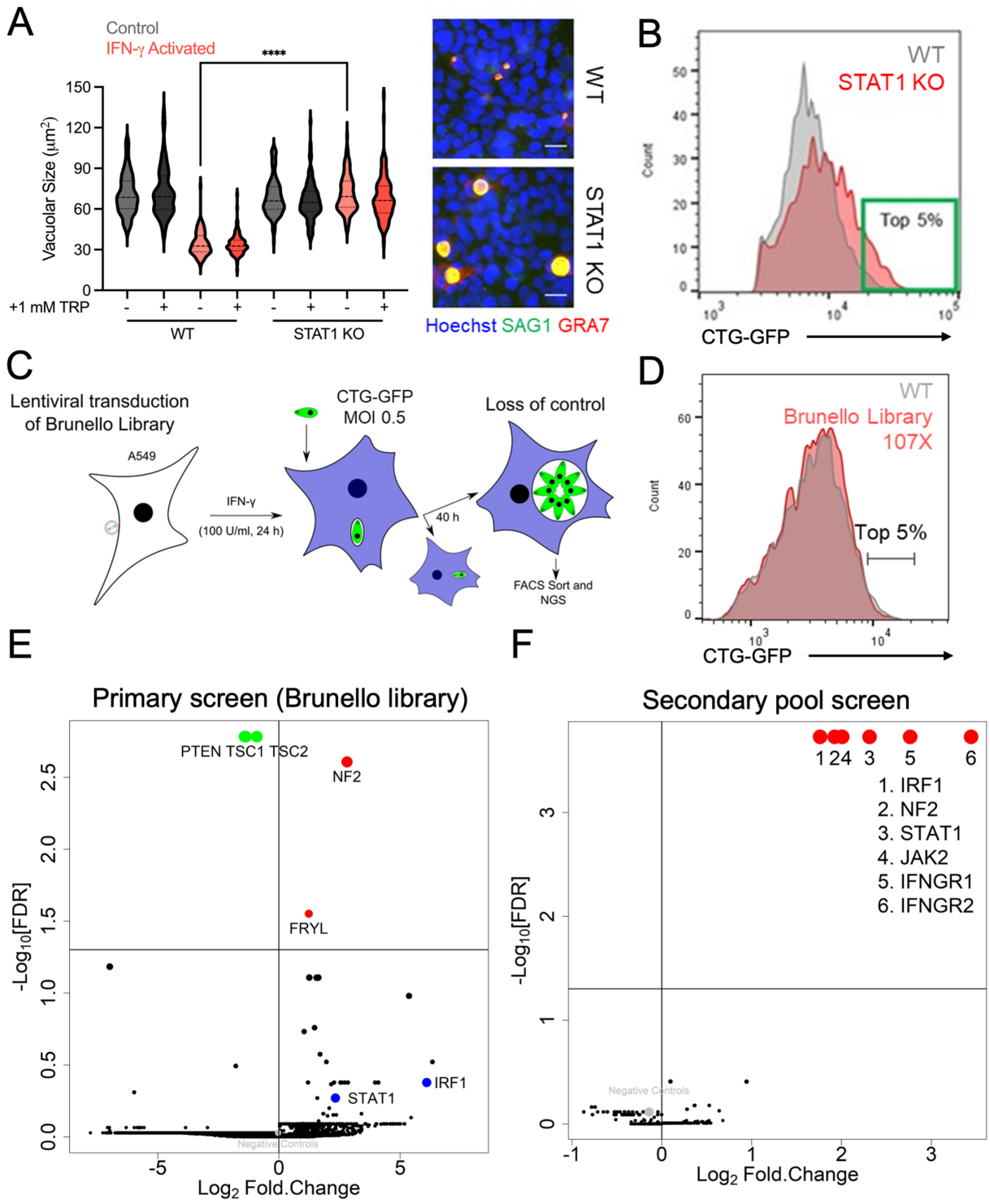

869

870 **Figure 1** Design and implementation of genome-wide CRISPR screens for loss of IFN-γ-
871 mediated parasite growth restriction in human cells (A) Tryptophan (TRP)-independent
872 restriction of *T. gondii* in lung alveolar epithelial A549 cells. Wild type (WT) and STAT1 knock

873 out (KO) A549 cells (**Fig. S1A**) were treated ± IFN-γ (100 Units/ml) 24 h prior to infection with
874 type III CTG strain of *T. gondii.* The cells were either left untreated (Control) or supplemented
875 with 1 mM TRP for 40 h. Growth was measured by vacuolar size (microns^2) for at least 3
876 biological replicates with ≥ 30 images per sample and replicate. Violin plot shows mean
877 vacuolar size per image with black bar representing the median. **** $P < 0.0001$ using unpaired
878 Two-tailed t-test with Welch's correction. Representative images of WT and STAT1 KO A549
879 cells (+IFN-γ +TRP) infected with CTG and analyzed at 40 h hpi. Nuclei labeled with Hoechst
880 (blue), parasites with anti-SAG1 (green) and the vacuole membrane with anti-GRA7 (red). Scale
881 bar = 20 microns. (B) IFN-γ activated WT vs. STAT1 KO A549 cells infected with CTG
882 expressing GFP (CTG-GFP) were fixed 40 hpi and analyzed by flow cytometry. Histogram
883 shows GFP positive (CTG-GFP infected) cells. Green box defines the top 5% of CTG-GFP
884 expressing cells. (C) Design of genome-wide CRISPR-Cas9 to identify factors involved in IFN-γ
885 mediated parasite growth restriction in human (A549) cells. (D) The Brunello library (36) was
886 transduced into A549 cells at ~100X coverage. Histogram of CTG-GFP infection analyzed at 40
887 hpi in IFN-γ activated control (WT) and Brunello library transduced A549 cells. (E) Primary
888 genome-wide CRISPR screen showing Log_2 fold change in sgRNAs from the top 5% of CTG-
889 GFP expressing cells (T5) compared to uninfected cells plotted against $-log_{10}$ false discovery
890 rate (FDR) for all 4 independent replicates combined. Genes for significantly enriched sgRNAs
891 (red) vs. significantly depleted sgRNAs in the T5 pool (green) are labeled. (F) Secondary
892 CRISPR screen consisting of a sub-pool of 224 genes that were significantly enriched in the T5
893 population (Log_2Fold Change > 1 and $P < 0.05$) in at least 2 out of the 4 replicates of the
894 primary Brunello screen (**Fig. S1B**). Log_2 Fold Change is plotted against $-log_{10}$ FDR for all 4
895 independent replicates combined.
896
897

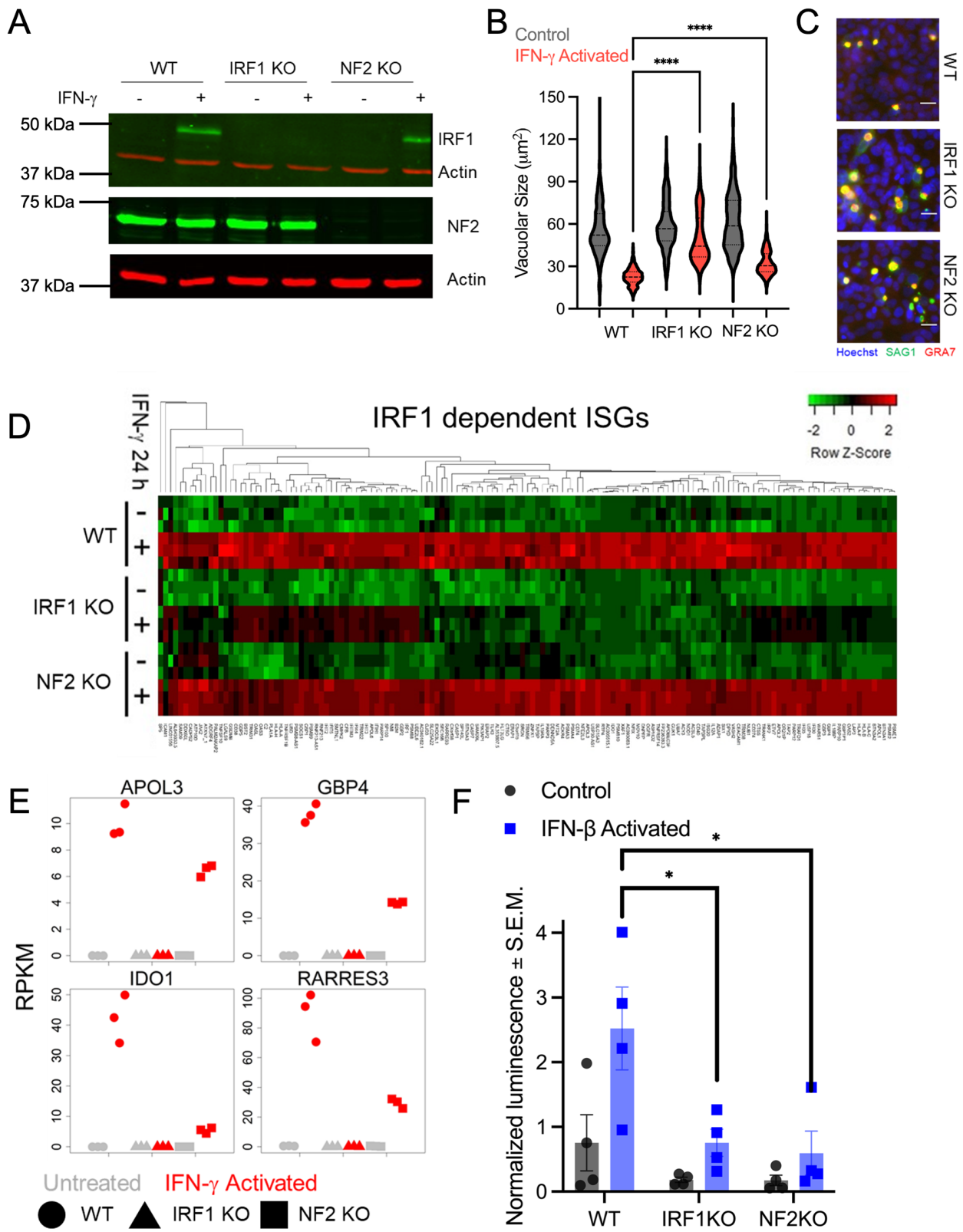

Figure 2 NF2 dampens IFN-γ-mediated growth restriction by inhibiting ISG induction. (A) Immunoblots for IRF-1 and NF2 in wild type, IRF1 KO, and NF2 KO A549 cells (**Fig. S2A and**

901 **S2B**). Actin was used as a loading control. (B) Wild type, IRF1 KO, and NF2 KO A549 cells
902 treated ± IFN-γ (100 U/ml) for 24 h, infected with CTG strain *T. gondii*, and evaluated for growth
903 restriction at 40 hpi. Violin plots show mean vacuolar size per image with the black bar
904 representing the median for at least 3 biological replicates containing at least 30 images per
905 sample and replicate. **** $P < 0.0001$ using Ordinary one-way ANOVA with Turkey's multiple
906 comparison test. (C) Representative images of IFN-γ activated wild type, IRF1 KO and NF2 KO
907 A549 cells infected with CTG and analyzed at 40 hpi. Cells were labelled with Hoechst for nuclei
908 (blue), anti-SAG1 for parasites (green), and anti-GRA7 for vacuoles (red). Scale bar = 20
909 microns. (D) Global transcriptional profiling from A549 cells treated ± IFN-γ (100 U/ml) for 24 h.
910 Heat maps depict genes that were induced in WT but not in IRF1 KO cells from 3 biological
911 replicates clustered using 1-Pearson distance and average linkage on normalized Log_2 (RPKM)
912 values. Normalized Z-scores are color-scaled from down-regulation (green) to upregulation
913 (red). (E) RPKM values showing partial induction of select ISGs in NF2 KO cells upon IFN-γ
914 activation compared to WT cells. (F) ISRE promoter activity from A549 cells transfected with
915 ISRE reporter plasmid expressing Gaussia luciferase (9) and control pCMV-Red Firefly Luc
916 plasmid (Thermo Fisher Scientific) for 24 h. Bar plot shows mean ± S.E.M Gaussia luciferase
917 activity normalized to firefly luciferase activity for 4 independent biological replicates. * $P < 0.05$
918 using Two-way ANOVA with Turkey's multiple comparison test.
919

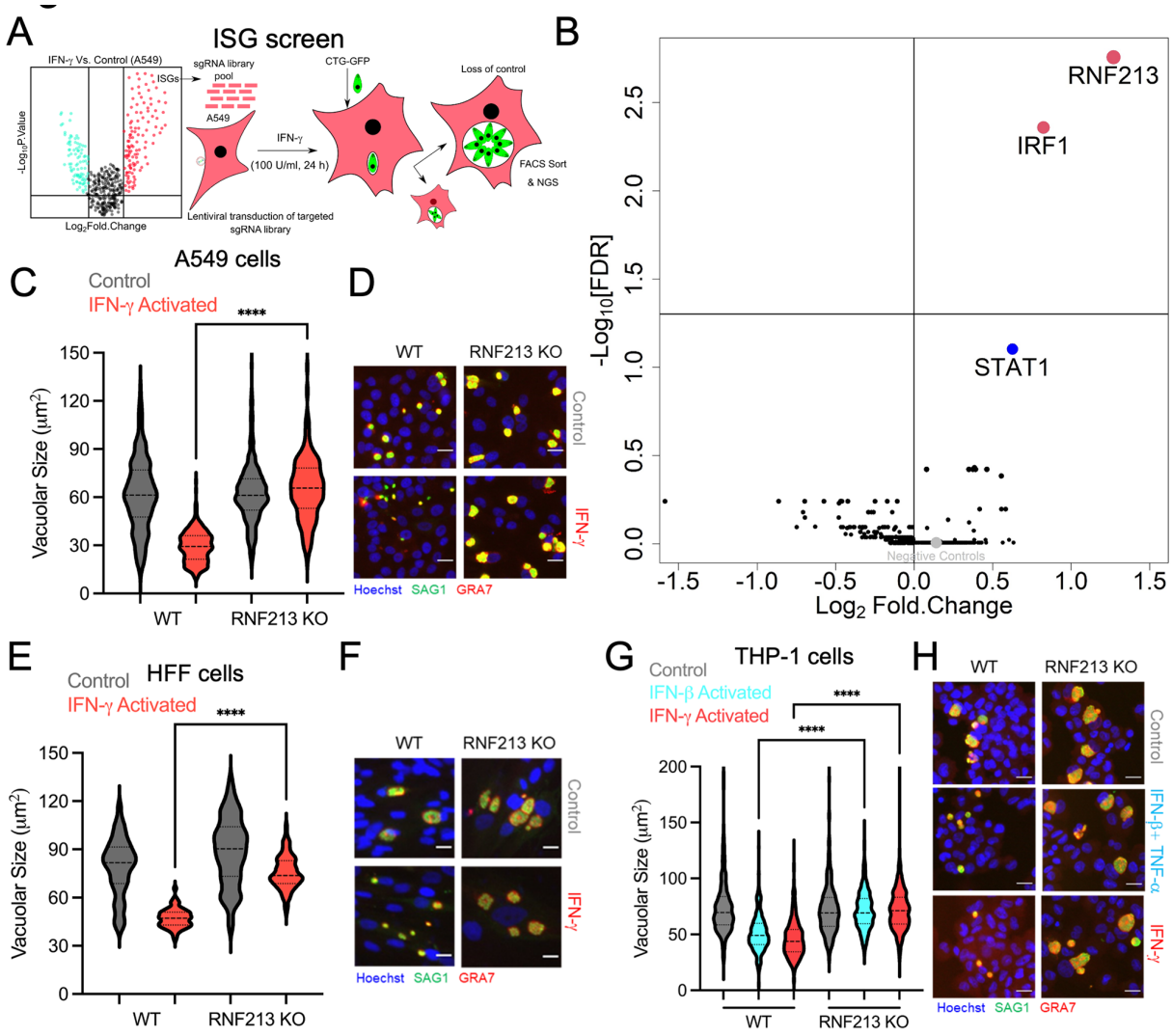

Figure 3 CRISPR-Cas9 screen identifies RNF213 as the primary ISG required for IFN-γ-mediated growth restriction of *T. gondii* in human cells (A) Design of ISG targeted sgRNA CRISPR-Cas9 screen using a sub-pool of ISGs that were previously shown to be upregulated in A549 cells treated with IFN-γ (34). (B) Targeted sgRNA screen of ISGs upregulated by IFN-γ identified two genes that were significantly depleted in the top 5% of CTG-GFP expressing cells (red). Log_2 Fold Change is plotted against $-log_{10}$ FDR for all 4 independent replicates combined. (C) Wild type and RNF213 KO A549 cells (**Fig. S4A and 4B**) treated ± IFN-g (100 U/ml) for 24 h, infected with CTG strain *T. gondii*, and evaluated for growth restriction by quantifying vacuolar size. Vacuolar growth of parasites was measured for at least 3 independent biological replicates with 30 images per sample and replicate. Violin plot shows mean vacuolar size per image with black bar representing the median. ****$P < 0.01$ using two-tailed unpaired Student's t-test with Welch's correction. (D) Representative images showing nuclei stained with Hoechst

933 (blue), parasites stained with anit-SAG1 (green), and the vacuole membrane stained with anti-
934 GRA7 (red). Scale bar = 20 microns. (E) Vacuolar growth of parasites at 40 hpi in ± IFN-γ
935 activated WT and RNF213 KO human foreskin fibroblast (HFF) cells. Violin plot shows mean
936 vacuolar size (μm^2) per image with black bar as median for at least 3 independent biological
937 replicates with at least 30 images per sample and replicate. **** $P < 0.0001$ two-tailed unpaired
938 Student's t-test with Welch's correction. (F) Representative images of the vacuole size in control
939 and IFN-γ activated WT and RNF213 KO HFF cells infected with CTG and analyzed at 40 hpi.
940 Nuclei were labelled with Hoechst (blue), the parasite with anti-SAG1 (green) and the vacuole
941 membrane with anti-GRA7 (red) with bar = 20 μm. (G) Vacuolar growth of parasites at 40 hpi in
942 control, IFN-β+TNF-α and IFN-γ activated WT and RNF213 KO human THP-1 macrophages.
943 Violin plot shows mean vacuolar size (μm^2) per image with black bar as median for at least 3
944 biological replicates with at least 30 images per sample and replicate. **** $P < 0.0001$ using
945 Ordinary one-way ANOVA with Turkey's multiple comparisons test. (H) Representative images
946 of control, IFN-β+TNF-α and IFN-γ activated WT and RNF213 KO THP-1 cells infected with
947 CTG and analyzed at 40 hpi. Nuclei are labelled with Hoechst (blue), parasites with anti-SAG1
948 (green) and the vacuole membrane with anti-GRA7 (red). Scale bar = 20 μm.
949

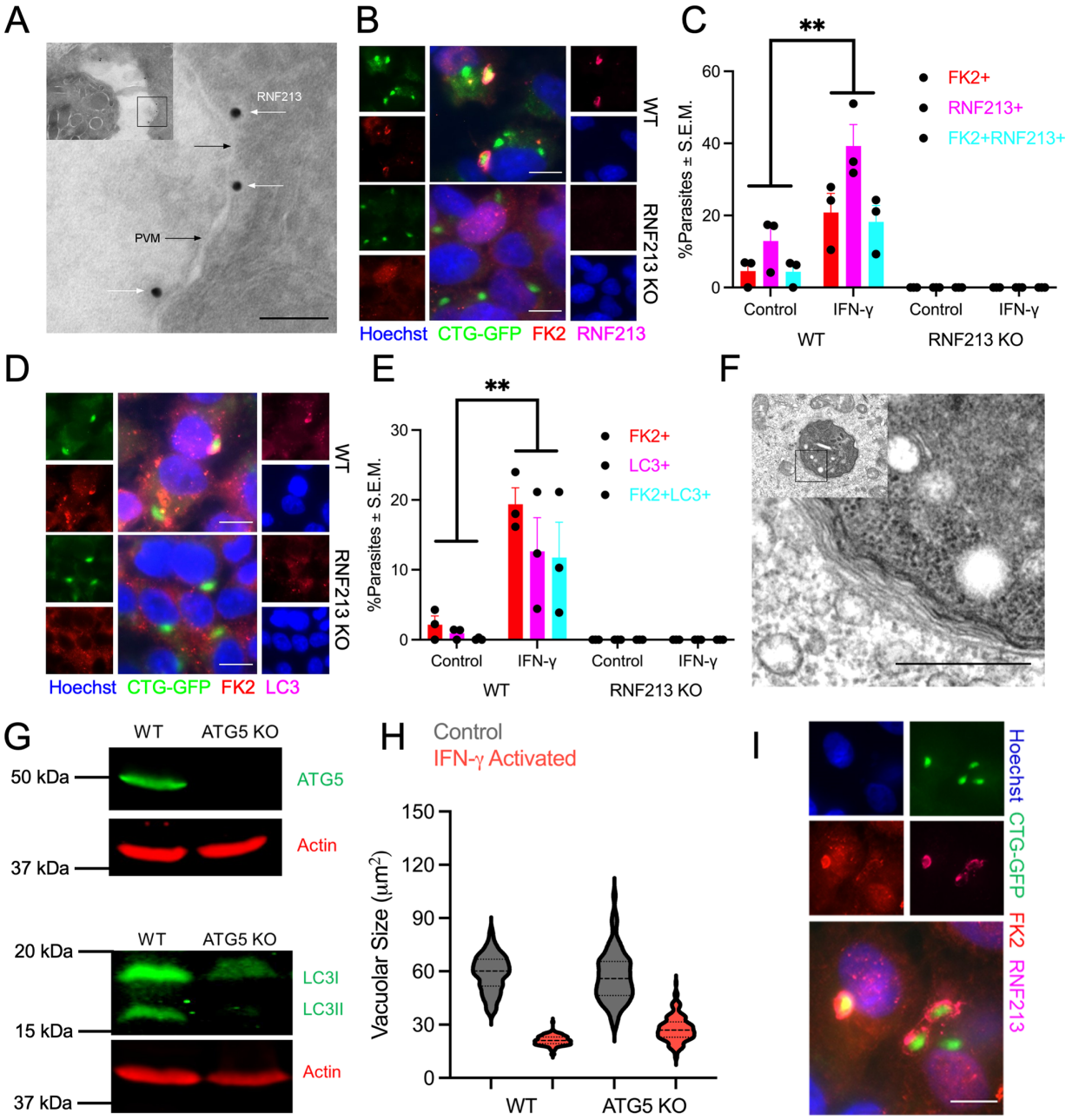

Figure 4 RNF213 co-localized with ubiquitinated parasite-containing vacuoles. (A) Immuno-EM labeling of RNF213 in IFN-γ activated wild type A549 cell infected with CTG parasite (inset) at 6 hpi. Parasite vacuolar membrane (PVM). Bar = 100 nm. (B) Representative images of WT and RNF213 KO A549 cells infected with CTG-GFP at 6 hpi. Cells were stained with FK2 (mono-poly ubiquitin; red) and anti-RNF213 (magenta). Nuclei were labelled with Hoechst (blue) and parasites were GFP labelled (green), Bar = 10 μm. (C) Quantification of FK2+ (red), RNF213+ (magenta) and FK2+RNF213+ (cyan) parasites for at least 3 biological replicates, mean ± S.E.M. ** $P < 0.01$ using Two-way ANOVA with Turkey's multiple comparisons test. (D)

959 Representative images of wild type and RNF213 KO A549 cells infected with CTG-GFP at 6 hpi.
960 The cells were stained with FK2 (red) and anti-LC3B (magenta). Nuclei were labelled with
961 Hoechst (blue) and parasites were GFP labelled (green). Scale bar = 10 μm. (E) Quantification
962 of FK2+ (red), LC3+ (magenta) and FK2+LC3+ (cyan) parasites for at least 3 biological
963 replicates, mean ± S.E.M. ** $P < 0.01$ using Two-way ANOVA with Turkey's multiple
964 comparisons test. (F) Transmission electron microscopic image of IFN-γ activated wild type
965 A549 cell infected with CTG parasite (inset) at 6 hpi. Wrapping by multiple membranes is
966 highlighted in the magnified view. Bar = 500 nm. (G) ATG5 (top) and LC3B (bottom)
967 immunoblots of WT and ATG5 KO A549 cells. Actin was used as loading control. (H) Vacuolar
968 growth of CTG parasite at 40 hpi in ± IFN-γ activated wild type and ATG KO cells. Violin plot
969 shows mean vacuolar size (μm^2) per image with black bar as median for an experiment with at
970 least 30 images per sample. (I) Representative image of IFN-γ activated ATG5 KO A549 cells
971 infected with CTG-GFP at 6 hpi. The cells are stained with FK2 (red) and anti-RNF213
972 (magenta). Bar = 10 μm.
973

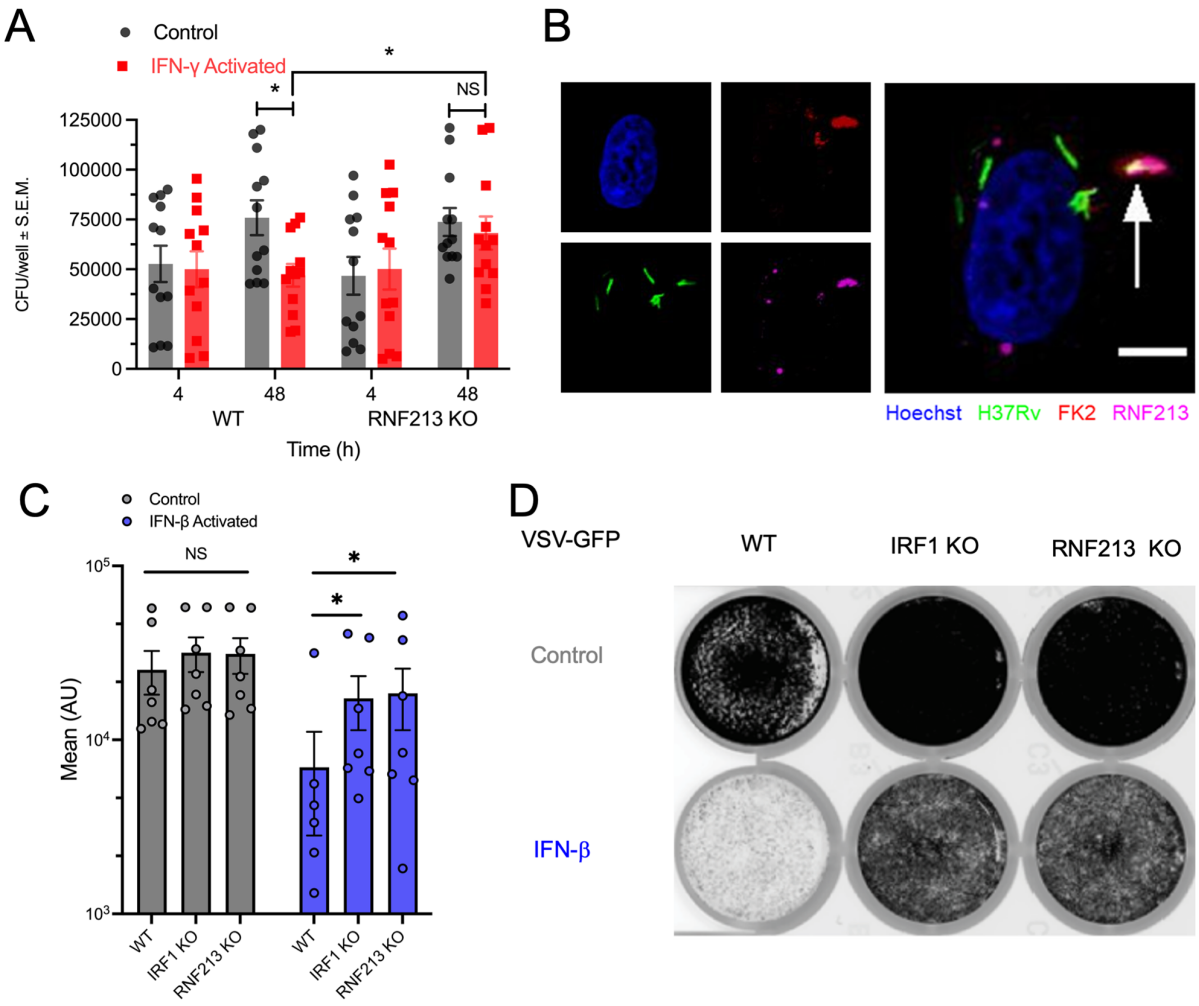

Figure 5 RNF213 is required for interferon-mediated control of intracellular bacterial and viral infection in human cells. (A) Mtb growth in ± IFN-γ (100 U/ml for 24 h) activated WT and RNF213 KO A549 cells at 4 and 48 hpi. Data shows mean colony forming units (CFU) per well ± S.E.M. from four independent experiments each with 3 internal replicates. * $P < 0.05$ using two-tailed unpaired Student's t-test. (B) Representative image showing co-localization of Mtb (green) with ubiquitin and RNF213. Cells were stained with FK2 (red) and RNF213 (magenta) in IFN-γ activated A549 cells that were analyzed at 8 hpi. Arrow depicts FK2+ and RNF213+ Mtb. Nuclei are labelled with Hoechst (blue). Scale bar = 5 μm. (C) Control and IFN-β (24 h, 100 U/ml) activated WT, IRF1 KO and RNF213 KO A549 cells infected with MOI 1 VSV-GFP (recombinant vesicular stomatitis virus expressing enhanced green fluorescent protein) at 24 hpi. Bar plot shows levels of GFP expression plotted as mean arbitrary units (AU). Data are means ± SEM for 7 independent biological replicates. * $P < 0.05$ using Two-way ANOVA with Dunnett's

987 multiple comparison test. (D) Representative images showing total GFP emission imaged by
988 Typhoon scanning of the 24-well plate.
989